

Trajectory-based Robustness Analysis for Nonlinear Systems

Peter Seiler and Raghu Venkataraman

Abstract

This paper considers the robustness of an uncertain nonlinear system along a finite-horizon trajectory. The uncertain system is modeled as a connection of a nonlinear system and a perturbation. The analysis relies on three ingredients. First, the nonlinear system is approximated by a linear time-varying (LTV) system via linearization along a trajectory. This linearization introduces an additional forcing input due to the nominal trajectory. Second, the input/output behavior of the perturbation is described by time-domain, integral quadratic constraints (IQCs). Third, a dissipation inequality is formulated to bound the worst-case deviation of an output signal due to the uncertainty. These steps yield a differential linear matrix inequality (DLMI) condition to bound the worst-case performance. The robustness condition is then converted to an equivalent condition in terms of a Riccati Differential Equation. This yields a computational method that avoids heuristics often used to solve DLMI, e.g. time gridding. The approach is demonstrated by a two-link robotic arm example.

I. INTRODUCTION

This paper develops theoretical and computational methods to analyze the robustness of uncertain nonlinear systems over finite time horizons. Motivating applications include robotic systems [1], space launch vehicles [2], [3], and aircraft during the landing phase [4]. The analysis in this paper considers an uncertain system modeled by an interconnection of a (nominal) nonlinear, time-varying system and an uncertainty. The uncertainty can model dynamic or parametric uncertainty. It can also model non-differentiable nonlinearities, e.g. saturation or deadzone. The input-output properties of the uncertainty are characterized by integral quadratic constraints

Email: peter.j.seiler@gmail.com

Email: veraghu@amazon.com.

This work was funded by Amazon.com Services LLC.

(IQCs) [5], [6]. The main result in [5] is an IQC stability theorem evaluated on an infinite time-horizon for the case where the nominal system is linear and time-invariant (LTI).

This paper makes two contributions. The first contribution is a theoretical condition to compute finite horizon robustness metrics for uncertain nonlinear systems. The objective is to assess the worst-case deviation from a nominal trajectory caused by the uncertainty. This analysis problem is approximated, via linearization along the trajectory, by the following problem: compute the worst-case \mathcal{L}_2 -norm for an output of an uncertain LTV system over the set of uncertainties (Section II). The uncertain LTV system includes a forcing due to the nominal trajectory. This forcing is addressed by using an augmented LTV system with a non-zero initial condition as done previously in [7], [8]. The main technical result (Theorem 1 in Section III) is a differential linear matrix inequality (DLMI) condition to bound the worst-case deviation. This theorem uses standard dissipation inequality and IQCs results.

The “tightest” bound on worst-case deviation can be computed by a convex optimization with DLMI constraints on a storage function matrix $P(t)$ and IQC variables. This involves infinite dimensional constraints due to dependence on t and a search over the space of differentiable functions for $P(t)$. A typical heuristic is to enforce the constraints on a finite time grid and use a finite-dimensional parameterization of $P(t)$ using basis functions. This heuristic has been used for both LTV [9], [10], [11], [8] and linear parameter varying (LPV) systems [12], [13]. However there are no formal guarantees, in general, with these approximations.

A second contribution of this paper is a computational algorithm to assess the worst-case deviation that avoids these heuristics (Section IV). We instead convert to an equivalent finite dimensional optimization. This step relies on a connection to Riccati Differential Equations (RDEs) using the LTV Bounded Real Lemma [14], [15], [16], [17], [18]. This connection can also be used to compute subgradients with minimal computational cost (Section IV-B). This builds on related prior work by [19], [20], [21]. As a result the ellipsoid algorithm can be used to solve the optimization to within a desired accuracy (Section IV-C). This is efficient if the IQC is parameterized by a small number of variables. The approach is demonstrated by analyzing the robustness of a two-link robot tracking a desired trajectory (Section V).

Finite-horizon robustness of continuous-time LTV systems has also been considered in [19], [20] and more recently in [9], [10], [11], [3]. There is also related work in discrete-time, e.g. [22], [23], [24]. These works mainly treat the uncertain LTV system as the starting point for the analysis. One exception is [8] which considers the effect of parametric uncertainty in a

nonlinear model. The work in [8] also uses linearization along a nominal trajectory. It uses the basis function/time gridding heuristic to compute bounds on the induced \mathcal{L}_2 gain of the uncertain LTV approximation from an exogenous disturbance to an output signal. Our paper is similar but we use a different formulation for the robustness metric and our computational algorithm avoids the use of heuristic time gridding and basis functions.

Notation: \mathbb{R}^n and \mathbb{C}^n denote the sets of n -by-1 real and complex vectors. $\mathbb{R}^{n \times m}$ and \mathbb{S}^n denote the sets of n -by- m real matrices and n -by- n real, symmetric matrices. The $\mathcal{L}_2^n[0, T]$ norm of a signal $v : [0, T] \rightarrow \mathbb{R}^n$ on a finite horizon $T < \infty$ is $\|v\|_{2,[0,T]} := \left(\int_0^T v(t)^\top v(t) dt \right)^{1/2}$. If $\|v\|_{2,[0,T]} < \infty$ then $v \in \mathcal{L}_2[0, T]$. The superscript n is omitted from $\mathcal{L}_2^n[0, T]$ when the dimension is clear.

II. PROBLEM FORMULATION

A. Uncertain Nonlinear System

Consider an uncertain system defined by the interconnection of a time-varying, nonlinear system G_{NL} and an uncertainty Δ as shown in Figure 1. The system G_{NL} is described by the following state-space model:

$$\begin{aligned} \dot{x}(t) &= f(x(t), w(t), d(t), t) \\ v(t) &= g_v(x(t), w(t), d(t), t) \\ e(t) &= g_e(x(t), w(t), d(t), t) \end{aligned} \tag{1}$$

where $x(t) \in \mathbb{R}^{n_x}$ is the state at time t . The inputs of G_{NL} at time t are $w(t) \in \mathbb{R}^{n_w}$ and $d(t) \in \mathbb{R}^{n_d}$ while $v(t) \in \mathbb{R}^{n_v}$ and $e(t) \in \mathbb{R}^{n_e}$ are outputs. The vector field $f : \mathbb{R}^{n_x \times n_w \times n_d \times 1} \rightarrow \mathbb{R}^{n_x}$ is assumed to be continuously differentiable. Similarly, the output mappings g_v and g_e are assumed to be continuously differentiable.

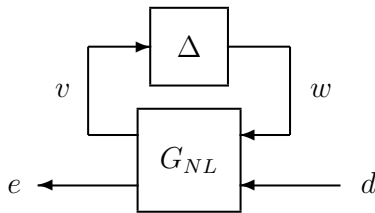


Fig. 1. Uncertain system defined by the interconnection of a time-varying nonlinear system G_{NL} and uncertainty Δ .

The uncertainty is a causal operator $\Delta : \mathcal{L}_2^{n_v}[0, T] \rightarrow \mathcal{L}_2^{n_w}[0, T]$ that maps v to w . It is assumed to be an element of a set $\mathbf{\Delta}$ of block-structured uncertainties as is standard in robust control [25]. The uncertainty $\Delta \in \mathbf{\Delta}$ can include blocks for unmodeled dynamics, parametric variations, and/or infinite dimensional operators (e.g. time delays). It can also include non-differentiable nonlinearities, e.g. saturations, that are separate from the differentiable nonlinearities in G_{NL} . The term ‘‘uncertainty’’ is used for simplicity when referring to Δ .

Next, assume an input $\bar{d} : [0, T] \rightarrow \mathbb{R}^{n_d}$ and initial condition $x(0) = \bar{x}_0$ are given. The nominal trajectory of the uncertain system is obtained when $\Delta = 0$. This yields $\bar{w}(t) = 0$ while the other nominal signals $(\bar{x}, \bar{v}, \bar{e})$, satisfy:

$$\begin{aligned}\dot{\bar{x}}(t) &= f(\bar{x}(t), 0, \bar{d}(t)) \\ \bar{v}(t) &= g_v(\bar{x}(t), 0, \bar{d}(t)) \\ \bar{e}(t) &= g_e(\bar{x}(t), 0, \bar{d}(t)).\end{aligned}\tag{2}$$

If $\Delta \neq 0$ then $w \neq 0$, in general. This will perturb the uncertain system from the nominal trajectory giving new signals (x, v, e) . These perturbed signals depend on the specific uncertainty $\Delta \in \mathbf{\Delta}$. We assume that the nominal solution exists on $[0, T]$ and also that the perturbed solutions exist on $[0, T]$ for all $\Delta \in \mathbf{\Delta}$. The objective is to bound (approximately) the worst-case deviation of the output signal in the $\mathcal{L}_2[0, T]$ norm: $\max_{\Delta \in \mathbf{\Delta}} \|e - \bar{e}\|_{2,[0,T]}$.

B. Linearization Along Trajectory

The approach taken here is to linearize the dynamics of G_{NL} around the nominal trajectory (assuming \bar{d} and \bar{x}_0 are fixed):

$$\begin{aligned}\dot{x}(t) &= \dot{\bar{x}}(t) + A(t)(x(t) - \bar{x}(t)) + B(t)w(t) \\ v(t) &= \bar{v}(t) + C_v(t)(x(t) - \bar{x}(t)) + D_{vw}(t)w(t) \\ e(t) &= \bar{e}(t) + C_e(t)(x(t) - \bar{x}(t)) + D_{ew}(t)w(t).\end{aligned}$$

The time-varying matrices are given by gradients evaluated along the nominal trajectory, e.g. $A(t) := \nabla_x f|_{(\bar{x}(t), 0, \bar{d}(t))}$. The linearization can be re-written in perturbation coordinates: $\delta_x := x - \bar{x}$, $\delta_v := v - \bar{v}$, and $\delta_e := e - \bar{e}$. This yields a linear time-varying (LTV) approximation,

G_{LTV} :

$$\begin{aligned}\dot{\delta}_x(t) &= A(t) \delta_x(t) + B(t) w(t) \\ \delta_v(t) &= C_v(t) \delta_x(t) + D_{vw}(t) w(t) \\ \delta_e(t) &= C_e(t) \delta_x(t) + D_{ew}(t) w(t).\end{aligned}\tag{3}$$

The uncertainty does not effect the initial condition, i.e. the perturbed and nominal trajectories have the same initial condition $x(0) = \bar{x}_0$. Hence the initial condition of G_{LTV} is $\delta_x(0) = 0$.

Figure 2 shows the linearized approximation for the original uncertain system. The nonlinear system G_{NL} is replaced by its linearization G_{LTV} . The nominal trajectory affects the linearized model in two ways. First, the state-matrices of (3) depend on (\bar{x}, \bar{d}) . Second, the input to Δ is $v = \bar{v} + \delta_v$ and includes forcing due to nominal input \bar{v} . If $\Delta \neq 0$ then the nominal signal \bar{v} will force G_{LTV} via w thus generating a perturbed output $\delta_e \neq 0$.

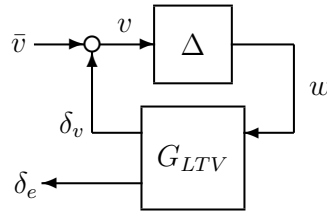


Fig. 2. Uncertain system defined by the interconnection of an LTV system G_{LTV} and uncertainty Δ including forcing due to \bar{v} .

The precise problem addressed by this paper is to compute a bound on the worst-case deviation for the uncertain system in Figure 2:

$$\max_{\Delta \in \mathbf{\Delta}} \|\delta_e\|_{2,[0,T]}\tag{4}$$

The analysis is based on the linearized model G_{LTV} . Hence it assumes that w is sufficiently small that the higher-order terms dropped in the linearization are negligible. It is possible to bound the effect of linearization errors as in [26], [8] but we will not do so here. Another assumption, implicit in Figure 1, is that the uncertainty Δ enters in a rational, i.e. feedback, form. This is sufficient for many types of unmodeled dynamics, delays, and non-differentiable nonlinearities. However, parametric uncertainty often appears in a non-rational form in a nonlinear model. Parametric uncertainties are treated in [8] via linearization along a nominal trajectory. The approach in [8] could be combined with the method in this paper but, again, this is not pursued.

III. WORST-CASE NORM

A. Augmented System

We'll focus on the worst-case analysis problem formulated in Section II-B with the linearized dynamics. The first step is to incorporate the effect of \bar{v} into an augmented LTV system with state $x_a := \begin{bmatrix} \delta_x \\ 1 \end{bmatrix} \in \mathbb{R}^{n_x+1}$. The linearized approximation in Figure 2 is equivalent to the interconnection of $w = \Delta(v)$ and the following LTV system:

$$\begin{aligned} \dot{x}_a(t) &= A_a(t)x_a(t) + B_a(t)w(t) \\ v(t) &= C_{v,a}(t)x_a(t) + D_{vw}(t)w(t) \\ \delta_e(t) &= C_{e,a}(t)x_a(t) + D_{ew}(t)w(t) \\ x_a(0) &= \begin{bmatrix} 0 \\ 1 \end{bmatrix}, \end{aligned} \tag{5}$$

where the augmented state matrices are defined as:

$$\begin{aligned} A_a(t) &:= \begin{bmatrix} A(t) & 0 \\ 0 & 0 \end{bmatrix}, \quad B_a(t) := \begin{bmatrix} B(t) \\ 0 \end{bmatrix}, \\ C_{v,a}(t) &:= \begin{bmatrix} C_v(t) & \bar{v} \end{bmatrix}, \quad C_{e,a}(t) := \begin{bmatrix} C_e(t) & 0 \end{bmatrix}. \end{aligned}$$

The augmented system (5), denoted G_a , has a non-zero initial condition. The definition of A_a and B_a ensure that the last (scalar) entry of x_a is identically equal to 1 for all solutions. Thus the output equation for $v(t)$ includes the effect of the nominal signal \bar{v} . This augmented state method was used in [7], [8] for similar trajectory-based linearizations. The offset \bar{v} is needed to ensure that the linearization provides an accurate approximation.

One technical issue is that the uncertain LTV system could be ill-posed. Specifically, $w = \Delta(v)$ and the output equation $v = C_{v,a}x_a + D_{vw}w$ may involve an algebraic equation. For example, if the uncertainty is a time-varying matrix $\Delta(t)$ then the algebraic equation at each time is:

$$(I - D_{vw}(t)\Delta(t))v(t) = C_{v,a}(t)x_a(t) \tag{6}$$

This algebraic equation will have no solutions or non-unique solutions if $(I - D_{vw}(t)\Delta(t))$ is singular. Such ill-posed cases can also occur when Δ is not necessarily a time-varying matrix. The uncertain system is said to be well-posed if such cases do not occur as formally defined next.

Definition 1. Consider the uncertain system defined by the interconnection of G_a in (5) and the set of causal uncertainties Δ . The uncertain system is well-posed if for each $\Delta \in \Delta$ there exists unique solutions $(x_a, v, w, \delta_e) \in \mathcal{L}_2^{n_x+1}[0, T]$ satisfying Equation (5) with $x_a(0) = \begin{bmatrix} 0 \\ 1 \end{bmatrix}$ and $w = \Delta(v)$.

B. Integral Quadratic Constraints (IQCs)

The next step is to bound the input/output behavior of $\Delta \in \Delta$. We will use the class of time-domain Integral Quadratic Constraints (IQCs) [5] defined below for this step.

Definition 2. A causal operator $\Delta : \mathcal{L}_2^{n_v}[0, T] \rightarrow \mathcal{L}_2^{n_w}[0, T]$ satisfies the time-domain IQC defined by $M \in \mathbb{S}^{n_v+n_w}$ if the following inequality holds $\forall v \in \mathcal{L}_2^{n_v}[0, T]$ and $w = \Delta(v)$:

$$\int_0^T \begin{bmatrix} v(t) \\ w(t) \end{bmatrix}^\top M \begin{bmatrix} v(t) \\ w(t) \end{bmatrix} dt \geq 0. \quad (7)$$

Time-domain IQCs can be used to bound the effect of various uncertainties [5]. For example, consider an uncertainty that is norm-bounded in the induced \mathcal{L}_2 norm: $\|\Delta\|_{2 \rightarrow 2} \leq \beta$ for some $\beta < \infty$. This uncertainty satisfies the IQC defined by $M = \begin{bmatrix} \beta^2 I & 0 \\ 0 & -I \end{bmatrix}$. As another example, a memoryless nonlinearity in the sector $[\alpha, \beta]$ satisfies the IQC defined by $M = \begin{bmatrix} -2\alpha\beta & \alpha+\beta \\ \alpha+\beta & -2 \end{bmatrix}$. An important point is that IQCs can be combined to form new IQCs. Suppose Δ satisfies the IQCs defined by $\{M_i\}_{i=1}^m \subset \mathbb{S}^{n_v+n_w}$. Then Δ also satisfies the IQC defined by $M(\lambda) := \sum_{i=1}^m \lambda_i M_i$ for any $\lambda_i \geq 0$.

Time domain IQCs, as defined above, are a special case of more general (and powerful) IQCs given in the literature. The integrand in (7) is a quadratic function of the input/output signals (v, w) . These are called non-dynamic IQCs. This is in contrast with dynamic IQCs that express the integrand as a quadratic function of filtered signals of (v, w) . Moreover, Definition 2 requires the constraint to hold over the finite time horizon $T > 0$. These are often referred to as hard IQCs [5]. This is in contrast to soft IQCs that only hold, in general, on an infinite horizon. The algorithm in this paper can be adapted to handle dynamic, hard IQCs with mainly notational changes.

C. Condition to Bound the Worst-Case Deviation

The next theorem gives a condition to bound the worst-case deviation $\max_{\Delta \in \Delta} \|\delta_e\|_{2,[0,T]}$. The proof uses IQCs and a standard dissipation argument [27], [28], [29], [30].

Theorem 1. Assume the uncertain system defined by the interconnection of G_a in (5) and the set of causal, uncertainties Δ is well-posed. Furthermore, assume each $\Delta \in \Delta$ satisfies the IQCs defined by $\{M_i\}_{i=1}^m \subset \mathbb{S}^{n_v+n_w}$.

If there exist non-negative scalars $\{\lambda_i\}_{i=1}^m$ and a differentiable function $P : [0, T] \rightarrow \mathbb{S}^{n_x+1}$ such that $P(T) \succeq 0$ and¹

$$\begin{aligned} & \begin{bmatrix} \dot{P} + A_a^\top P + P A_a & P B_a \\ B_a^\top P & 0 \end{bmatrix} + (\cdot)^\top \begin{bmatrix} C_{a,e} & D_{ew} \end{bmatrix} \\ & + \sum_{i=1}^m \lambda_i (\cdot)^\top M_i \begin{bmatrix} C_{a,v} & D_{vw} \\ 0 & I \end{bmatrix} \prec 0 \quad \forall t \in [0, T] \end{aligned} \quad (8)$$

then

$$\max_{\Delta \in \Delta} \|\delta_e\|_{2,[0,T]} \leq \left[\begin{bmatrix} 0 \\ 1 \end{bmatrix}^\top P(0) \begin{bmatrix} 0 \\ 1 \end{bmatrix} \right]^{\frac{1}{2}}. \quad (9)$$

Proof. Define a storage function $V : \mathbb{R}^{n_x+1} \times \mathbb{R} \rightarrow \mathbb{R}$ by $V(x_a, t) := x_a^\top P(t) x_a$. Consider any $\Delta \in \Delta$. By well-posedness, the uncertain system with Δ and $x_a(0) = \begin{bmatrix} 0 \\ 1 \end{bmatrix}$ has a unique solution (x_a, v, w, δ_e) . Left and right multiply (8) by $[x_a^\top, w^\top]$ and its transpose to show that V satisfies the dissipation inequality $\forall t \in [0, T]$:

$$\dot{V} + \delta_e^\top \delta_e + \sum_{i=1}^m \lambda_i \begin{bmatrix} v \\ w \end{bmatrix}^\top M_i \begin{bmatrix} v \\ w \end{bmatrix} \leq 0$$

Integrate over $[0, T]$ to obtain:

$$\begin{aligned} & V(x_a(T), T) - V(x_a(0), 0) + \|\delta_e\|_{2,[0,T]}^2 \\ & + \sum_{i=1}^m \lambda_i \int_0^T \begin{bmatrix} v(t) \\ w(t) \end{bmatrix}^\top M_i \begin{bmatrix} v(t) \\ w(t) \end{bmatrix} dt \leq 0. \end{aligned}$$

Apply $P(T) \succeq 0$, $x_a(0) = \begin{bmatrix} 0 \\ 1 \end{bmatrix}$, and the IQCs defined by $\{M_i\}_{i=1}^m$ to conclude:

$$\|\delta_e\|_{2,[0,T]}^2 \leq \begin{bmatrix} 0 \\ 1 \end{bmatrix}^\top P(0) \begin{bmatrix} 0 \\ 1 \end{bmatrix}. \quad (10)$$

This inequality holds for all $\Delta \in \Delta$ and hence this yields the bound in (9). \square

The inequality in Equation 8 is compactly denoted as $DLMI(t, P, \lambda) \prec 0$. This notation emphasizes that the constraint is a time-dependent, differential linear matrix inequality (DLMI)

¹The notation $(\cdot)^\top$ in (8) corresponds to a factor that can be determined from symmetry and hence is omitted.

in (P, λ) . The dependence on the state matrices of G_a and the IQC matrices $\{M_i\}_{i=1}^n$ is not explicitly denoted but will be clear from context.

The tightest upper bound on the worst-case deviation, based on Theorem 8, is obtained by solving the following optimization:

$$\begin{aligned} J^* &= \min_{\lambda \geq 0, P} \begin{bmatrix} 0 \\ 1 \end{bmatrix}^\top P(0) \begin{bmatrix} 0 \\ 1 \end{bmatrix} & (11) \\ \text{subject to: } & P(T) \succeq 0, \\ & DLMI(t, P, \lambda) \prec 0 \quad \forall t \in [0, T] \end{aligned}$$

The worst-case deviation is upper bounded by $\sqrt{J_{bnd}}$. The optimization involves convex constraints on the optimization variables λ and P . Moreover, the cost is a linear (and hence convex) function of P . Thus Equation 11 is a (convex) semidefinite program (SDP). However, there are two main issues with solving this optimization. First, the DLMI corresponds to an infinite number of constraints since it must hold for all $t \in [0, T]$. Second, the optimization requires a search over the space of differentiable functions $P : [0, T] \rightarrow \mathbb{S}^{n_x+1}$. A heuristic approach to approximately solve this optimization involves [9], [11], [8]: (i) enforcing the DLMI on a finite time grid, and (ii) restricting P to a linear combination of differentiable basis functions. These approximations yield a finite dimensional optimization but provides no guarantees on the solution accuracy.

IV. COMPUTATIONAL ALGORITHM

This section presents a computational method to convert the optimization (11) to an equivalent finite-dimensional optimization. This enables solutions via cutting plane methods without resorting to time-gridding or basis functions.

A. Finite-Dimensional Optimization

The first step is to define a function J involving the minimization over P for a fixed $\lambda \in \mathbb{R}^m$:

$$\begin{aligned} J(\lambda) &:= \min_P \begin{bmatrix} 0 \\ 1 \end{bmatrix}^\top P(0) \begin{bmatrix} 0 \\ 1 \end{bmatrix} & (12) \\ \text{subject to: } & P(T) \succeq 0, \\ & DLMI(t, P, \lambda) \prec 0 \quad \forall t \in [0, T] \end{aligned}$$

If the optimization is infeasible for a given λ then $J(\lambda) = +\infty$. Define the domain of J as $\mathcal{D} := \{\lambda \in \mathbb{R}^m : J(\lambda) < \infty\}$. It follows from the linear constraints and cost of (12) that $J : \mathcal{D} \rightarrow \mathbb{R}$ is a convex function and the domain \mathcal{D} is a convex set. The infinite dimensional optimization (11) can re-written in terms of J as follows:

$$J^* = \min_{\lambda \in \mathcal{D}, \lambda \geq 0} J(\lambda) \quad (13)$$

Equation 13 is, formally, a finite-dimensional convex optimization with decision variables $\lambda \in \mathbb{R}^m$. However, evaluating definition of J in (12) still involves a minimization over P with the time-dependent DLMI constraint.

Next, we show that $J(\lambda)$ can be evaluated directly without explicitly performing the minimization over P . To simplify notation, consider the DLMI in (8) and define (Q, S, R) as follows:

$$\begin{bmatrix} Q & S \\ S^\top & R \end{bmatrix} := \begin{bmatrix} Q_0 & S_0 \\ S_0^\top & R_0 \end{bmatrix} + \sum_{i=1}^m \lambda_i \begin{bmatrix} Q_i & S_i \\ S_i^\top & R_i \end{bmatrix} \quad (14)$$

where:

$$\begin{aligned} \begin{bmatrix} Q_0 & S_0 \\ S_0^\top & R_0 \end{bmatrix} &:= \begin{bmatrix} C_{a,e}^\top \\ D_{ew}^\top \end{bmatrix} [C_{a,e} \ D_{ew}] \\ \begin{bmatrix} Q_i & S_i \\ S_i^\top & R_i \end{bmatrix} &:= \begin{bmatrix} C_{a,v} & D_{vw} \\ 0 & I \end{bmatrix}^\top M_i \begin{bmatrix} C_{a,v} & D_{vw} \\ 0 & I \end{bmatrix}. \end{aligned} \quad (15)$$

The matrices are defined by the appropriate block partitioning. Here (Q, S, R) are functions of (t, λ) and $\{(Q_i, S_i, R_i)\}_{i=1}^m$ are only functions of t . The DLMI in (8) can thus be expressed as:

$$\begin{bmatrix} \dot{P} + A_a^\top P + P A_a & P B_a \\ B_a^\top P & 0 \end{bmatrix} + \begin{bmatrix} Q & S \\ S^\top & R \end{bmatrix} \prec 0 \quad (16)$$

The matrices in the DLMI can be used to define a related Riccati Differential Equation (RDE):

$$\begin{aligned} \dot{Y} + A_a^\top Y + Y A_a + Q \\ - (Y B_a + S) R^{-1} (Y B_a + S)^\top = 0 \end{aligned} \quad (17)$$

This is compactly denoted as $RDE(t, Y, \lambda) = 0$. The next theorem states that $J(\lambda)$ can be evaluated from the solution to this RDE.

Theorem 2. *Assume (A_a, B_a, Q, R, S) are all continuous functions of time. Moreover, assume $\lambda \in \mathbb{R}^m$ is given and $R(t, \lambda) < 0$ for all $t \in [0, T]$. Then the following are equivalent:*

- 1) $\lambda \in \mathcal{D}$, i.e. $J(\lambda) < \infty$.
- 2) There exists a differentiable function $P : [0, T] \rightarrow \mathbb{S}^{n_x+1}$ that satisfies $P(T) \succeq 0$ and $DLMI(t, P, \lambda) \prec 0$ for all $t \in [0, T]$.
- 3) There exists a differentiable function $Y : [0, T] \rightarrow \mathbb{S}^{n_x+1}$ that satisfies $Y(T) = 0$ and $RDE(t, Y, \lambda) = 0$ for all $t \in [0, T]$.

Moreover, if the conditions hold then:

$$J(\lambda) = \begin{bmatrix} 0 \\ 1 \end{bmatrix}^\top Y(0) \begin{bmatrix} 0 \\ 1 \end{bmatrix}. \quad (18)$$

Proof. The equivalence of 1 and 2 is a consequence of the definition of J in (12). The remainder of the proof shows that 2 and 3 are equivalent.

Condition 2 holds if and only if there exists $\epsilon_1 > 0$ such that the following Riccati Differential Inequality (RDI) holds for all $t \in [0, T]$:

$$\begin{aligned} \dot{P} + A_a^\top P + P A_a + Q \\ - (P B_a + S) R^{-1} (P B_a + S)^\top + \epsilon_1 \cdot I \prec 0 \end{aligned} \quad (19)$$

This follows from the Schur complement lemma [31] and $R(t, \lambda) < 0$.² The Bounded Real Lemma for LTV systems [14], [15], [16], [17], [18] states that there exists a differentiable function P satisfying $P(T) \succeq 0$ and (19) if and only if Condition 3 holds. The precise version of the LTV Bounded Real Lemma used here is Theorem 1 in [10], [11].

To conclude the proof we assume the conditions hold and show (18) is true. As noted above, if P satisfies the DLMI then P satisfies the RDI in (19). Thus there exists $W : [0, T] \rightarrow \mathbb{S}^{n_x+1}$ such that $W(t) \prec 0$ for all $t \in [0, T]$ and:

$$\begin{aligned} \dot{P} + A_a^\top P + P A_a + Q \\ - (P B_a + S) R^{-1} (P B_a + S)^\top = W \quad \forall t \in [0, T] \end{aligned} \quad (20)$$

This is an RDE with a perturbation W on the right side. We denote (20) by $RDE(t, P, \lambda) = W$. It follows from Lemma 1 in the Appendix that $P(0) \succeq Y(0)$. This inequality holds for any P that satisfies Condition 2 so that $J(\lambda) \geq \begin{bmatrix} 0 \\ 1 \end{bmatrix}^\top Y(0) \begin{bmatrix} 0 \\ 1 \end{bmatrix}$.

²The interval $[0, T]$ is compact since $T < \infty$. Hence a strict matrix inequality $M(t) < 0 \forall t \in [0, T]$ holds if and only if $\exists \epsilon_1 > 0$ such that $M(t) + \epsilon_1 \cdot I < 0 \forall t \in [0, T]$.

Next, if P satisfies Condition 2 then it satisfies the RDI in (19). This implies (via the equivalence of Conditions 2 and 3 to this perturbed RDI) that there exists a differentiable function $Y_1 : [0, T] \rightarrow \mathbb{S}^{n_x+1}$ that satisfies $Y_1(T) = 0$ and $RDE(t, Y_1, \lambda) = -\epsilon_1 \cdot I$. Define $\epsilon_k = \frac{1}{k}\epsilon_1$ for $k = 2, 3, \dots$ and let $Y_k : [0, T] \rightarrow \mathbb{S}^{n_x+1}$ be the solution to $Y_k(T) = 0$ and $RDE(t, Y_k, \lambda) = -\epsilon_k \cdot I$. It follows from Lemma 2 in the Appendix that $\lim_{k \rightarrow \infty} \|Y_k(0) - Y(0)\| = 0$. Moreover, each $\{Y_k\}_{k=1}^\infty$ satisfies the DLMI by the Schur complement lemma. Thus the optimization in (12) has feasible points arbitrarily close to $Y(0)$ and hence $J(\lambda) = \begin{bmatrix} 0 \\ 1 \end{bmatrix}^\top Y(0) \begin{bmatrix} 0 \\ 1 \end{bmatrix}$. \square

B. Subgradients

By Theorem 2, J can be evaluated directly from the solution of a RDE. There is no need to approximate the optimization by enforcing the DLMI on a time grid and using bases functions for P . This section demonstrates that subgradients on J can be computed with small additional computation. The subgradients are evaluated based on a linear quadratic (LQ) optimization defined in terms of (Q, S, R) from (14):

$$\begin{aligned} & \max_{w \in \mathcal{L}_2[0, T]} \int_0^T \begin{bmatrix} x_a(t) \\ w(t) \end{bmatrix}^\top \begin{bmatrix} Q(t, \lambda) & S(t, \lambda) \\ S(t, \lambda)^\top & R(t, \lambda) \end{bmatrix} \begin{bmatrix} x_a(t) \\ w(t) \end{bmatrix} dt \\ & \text{subject to: } \dot{x}_a = A_a x_a + B_a w, \quad x_a(0) = \begin{bmatrix} 0 \\ 1 \end{bmatrix} \end{aligned} \quad (21)$$

The next theorem is a variation of the cutting plane results in [19], [21].

Theorem 3. *If $\lambda \in \mathcal{D}$ then:*

- 1) *The optimal cost for (21) is equal to $J(\lambda)$.*
- 2) *The optimal cost is achieved by (x_a^*, w^*) satisfying the following with $x_a^*(0) = \begin{bmatrix} 0 \\ 1 \end{bmatrix}$:*

$$\begin{aligned} \dot{x}_a^* &:= \left(A_a - B_a R^{-1} (Y B_a + S)^\top \right) x_a \\ w^* &:= -R^{-1} (Y B_a + S)^\top x_a^*, \end{aligned} \quad (22)$$

where Y is the solution to $RDE(t, Y, \lambda) = 0$ with $Y(T) = 0$.

- 3) *J satisfies the subgradient inequality:*

$$J(\alpha) \geq J(\lambda) + g^\top (\alpha - \lambda) \quad \forall \alpha \in \mathbb{R}^m \quad (23)$$

where $g \in \mathbb{R}^m$ is defined by:

$$g_i := \int_0^T \begin{bmatrix} x_a^*(t) \\ w^*(t) \end{bmatrix}^\top \begin{bmatrix} Q_i(t) & S_i(t) \\ S_i(t)^\top & R_i(t) \end{bmatrix} \begin{bmatrix} x_a^*(t) \\ w^*(t) \end{bmatrix} dt \quad (24)$$

Proof. By Theorem 2, if $\lambda \in \mathcal{D}$ then there exists a solution Y to the RDE with boundary condition $Y(T) = 0$. Moreover, $J(\lambda) = \begin{bmatrix} 0 \\ 1 \end{bmatrix}^\top Y(0) \begin{bmatrix} 0 \\ 1 \end{bmatrix}$. It is a standard result in LQ optimal control that the optimal cost to (21) is $\begin{bmatrix} 0 \\ 1 \end{bmatrix}^\top Y(0) \begin{bmatrix} 0 \\ 1 \end{bmatrix}$ achieved by (x_a^*, w^*) as defined in Statement 2. See Chapter 2 of [32] or Proposition 8 of [19].

Next, consider Statement 3. If $\alpha \notin \mathcal{D}$ then $J(\alpha) = \infty$ and hence (23) holds trivially. Thus consider $\alpha \in \mathcal{D}$. The pair (x_a^*, w^*) is optimal for the LQ optimization defined with λ . It provides a lower bound on the maximal cost of the LQ optimization defined by any other $\alpha \in \mathcal{D}$:

$$J(\alpha) \geq \int_0^T \begin{bmatrix} x_a^*(t) \\ w^*(t) \end{bmatrix}^\top \begin{bmatrix} Q(t, \alpha) & S(t, \alpha) \\ S(t, \alpha)^\top & R(t, \alpha) \end{bmatrix} \begin{bmatrix} x_a^*(t) \\ w^*(t) \end{bmatrix} dt \quad (25)$$

Finally, it follows from the definition of Q in (14) that $Q(t, \alpha) = Q(t, \lambda) + \sum_{i=1}^m (\alpha_i - \lambda_i) Q_i$. Similar relationships hold for S and R . Thus (25) can be equivalently written as (23). \square

By Theorem 3, a subgradient for J at $\lambda \in \mathcal{D}$ can be evaluated using the solution Y of the RDE. First, the signals (x_a^*, w^*) are obtained by solving the dynamics (22) from the initial condition $x_a^*(0) = \begin{bmatrix} 0 \\ 1 \end{bmatrix}$. Second, the subgradient g is then obtained by performing the integrals in (24). These two steps have a small computational cost relative to cost of solving the RDE itself.

If $\lambda \notin \mathcal{D}$ then we can also construct a $g \in \mathbb{R}^m$ that separates λ from the feasible set \mathcal{D} [19], [21]. The construction is summarized here. If $\lambda \notin \mathcal{D}$ then the RDE does not have a solution on $[0, T]$. Specifically, the solution Y to $RDE(Y, t, \lambda) = 0$ grows unbounded when integrated backward from $Y(T) = 0$. Thus the solution exists only $(t_0, T]$ for some $t_0 \in (0, T)$. In this case, there exists non-trivial signals (x_a^*, w^*) on $[t_0, T]$ that satisfy:

$$\int_{t_0}^T \begin{bmatrix} x_a^*(t) \\ w^*(t) \end{bmatrix}^\top \begin{bmatrix} Q(t, \lambda) & S(t, \lambda) \\ S(t, \lambda)^\top & R(t, \lambda) \end{bmatrix} \begin{bmatrix} x_a^*(t) \\ w^*(t) \end{bmatrix} dt = 0 \quad (26)$$

$$\dot{x}_a^* = A_a x_a^* + B_a w^* \quad \text{with } x_a(t_0) = 0$$

A numerical implementation for this construction is given in [33].³ We can use this pair (x_a^*, w^*)

³Briefly, integrate Y backward to $Y(t_0 + \epsilon)$ for some sufficiently small $\epsilon > 0$. Let ρ_ϵ be the spectral radius of $Y(t_0 + \epsilon)$ and note that $\rho_\epsilon \rightarrow \infty$ as $\epsilon \rightarrow 0$. Let v_ϵ be the corresponding eigenvector of $Y(t_0 + \epsilon)$ associated with ρ_ϵ . Solve the dynamics (22) with initial condition $x_a^*(0) = \rho_\epsilon^{-1} v_\epsilon$ to obtain (x_a^*, w^*) .

to construct g from (24). By linearity, this pair satisfies the following for any $\alpha \in \mathbb{R}^m$:

$$\begin{aligned} \int_{t_0}^T \begin{bmatrix} x_a^*(t) \\ w^*(t) \end{bmatrix}^\top \begin{bmatrix} Q(t,\alpha) & S(t,\alpha) \\ S(t,\alpha)^\top & R(t,\alpha) \end{bmatrix} \begin{bmatrix} x_a^*(t) \\ w^*(t) \end{bmatrix} dt \\ = g^\top (\alpha - \lambda) \end{aligned}$$

Thus if $g^\top (\alpha - \lambda) \geq 0$ then (x_a^*, w^*) are non-trivial signals that yield non-negative LQ cost from $x_a^*(0) = 0$. The RDE fails to exist in this case by the LTV Bounded Real Lemma (Theorem 1 in [11]). Hence the feasible set satisfies $\mathcal{D} \subset \{\alpha : g^\top (\alpha - \lambda) < 0\}$. In other words, g defines a hyperplane that separates $\lambda \notin \mathcal{D}$ from the feasible set \mathcal{D} .

C. Solution Via Ellipsoidal Algorithm

Assume the convex optimization (13), $\min_{\lambda \in \mathcal{D}, \lambda \geq 0} J(\lambda)$, is feasible with optimal point λ^* and optimal cost $J^* = J(\lambda^*)$. Algorithm 1 provides pseudo-code to solve this using the ellipsoidal algorithm (Section 14.4 of [34]).

The algorithm computes a sequence of ellipsoids defined with a center $\lambda \in \mathbb{R}^n$ and shape matrix $\Lambda \succ 0$ as follows:

$$\mathcal{E}(\Lambda, \lambda) := \{\alpha \in \mathbb{R}^n : (\alpha - \lambda)^\top \Lambda^{-1} (\alpha - \lambda) \leq 1\}$$

The algorithm is initialized with a sphere of radius $R > 0$ centered at the origin: $\Lambda^{(0)} = R^2 \cdot I$ and $\lambda^{(0)} = 0$. Assume that $\lambda^* \in \Lambda^{(0)}$.

For each step $k = 0, 1, \dots$, the cost is evaluated at the ellipsoid center $J(\lambda^{(k)})$. Moreover, a vector $g^{(k)} \in \mathbb{R}^n$ is computed that is either a subgradient at $\lambda^{(k)}$, if feasible, or separates $\lambda^{(k)}$ from the infeasible set. Additional details on the computation of $g^{(k)}$ are given below. The optimal point lies in the intersection of $\mathcal{E}(\Lambda^{(k)}, \lambda^{(k)})$ and the half space $\mathcal{H}(g^{(k)}, \lambda^{(k)}) := \{\alpha : (g^{(k)})^\top (\alpha - \lambda^{(k)}) < 0\}$.

The ellipsoid algorithm computes the smallest ellipsoid that contains $\mathcal{E}(\Lambda^{(k)}, \lambda^{(k)}) \cap \mathcal{H}(g^{(k)}, \lambda^{(k)})$. The updated ellipsoid is defined in terms of the normalized vector $\tilde{g} := \frac{1}{\sqrt{(g^{(k)})^\top \Lambda g^{(k)}}} g^{(k)}$:

$$\begin{aligned} \lambda^{(k+1)} &:= \lambda^{(k)} - \frac{1}{m+1} \Lambda^{(k)} \tilde{g} \\ \Lambda^{(k+1)} &:= \frac{m^2}{m^2 - 1} \left(\Lambda^{(k)} - \frac{2}{m+1} \Lambda^{(k)} \tilde{g} \tilde{g}^\top \Lambda^{(k)} \right) \end{aligned} \tag{27}$$

If $\lambda^* \in \mathcal{E}(\Lambda^{(0)}, \lambda^{(0)})$ then the optimal point remains in the ellipsoid at each iteration. In addition, if $\lambda^{(k)}$ is feasible then the optimality gap is bounded by:

$$J(\lambda^{(k)}) - J^* \leq J_{\text{bd}} \quad (28)$$

where $J_{\text{bd}} := \sqrt{(g^{(k)})^\top \Lambda^{(k)} g^{(k)}}$

The ellipsoids shrink by a fixed factor $e^{-\frac{1}{2m}}$ at each iteration. If the optimization (13) is feasible and $\lambda^* \in \mathcal{E}(\Lambda^{(0)}, \lambda^{(0)})$ then the algorithm converges $J(\lambda^{(k)}) \rightarrow J^*$. Details for these facts are given in Section 14.4 of [34].

Finally, we discuss the construction of $g^{(k)}$ based on three possible cases:

- *Case 1:* The current ellipsoid center $\lambda^{(k)}$ has at least one negative entry, $\lambda_i^{(k)} < 0$ for some i . Thus the ellipsoid center is infeasible as it does not satisfy $\lambda^{(k)} \geq 0$. In this case $J(\lambda^{(k)}) = +\infty$ and any feasible point must satisfy $\alpha_i \geq 0 > \lambda_i^{(k)}$. Set $g^{(k)} = -e_i$ where $e_i \in \mathbb{R}^m$ is the i^{th} basis vector. Thus the feasible set lies in the half space $\mathcal{H}(g^{(k)}, \lambda^{(k)})$.
- *Case 2:* If the current ellipsoid center satisfies $\lambda^{(k)} \geq 0$ then integrate the RDE backward from $Y(T) = 0$. If the solution exists on $[0, T]$ then $J(\lambda^{(k)}) = \begin{bmatrix} 0 \\ 1 \end{bmatrix}^\top Y(0) \begin{bmatrix} 0 \\ 1 \end{bmatrix}$. Moreover, a subgradient $g^{(k)}$ can be computed from Theorem 3. The set of feasible points with strictly lower cost lies in $\mathcal{H}(g^{(k)}, \lambda^{(k)})$.
- *Case 3:* Suppose the current ellipsoid center satisfies $\lambda^{(k)} \geq 0$ but the RDE fails to exist on $[0, T]$. Then the ellipsoid center is infeasible because $\lambda^{(k)} \notin \mathcal{D}$. As discussed in Section IV-B, a separating hyperplane $g^{(k)}$ can be constructed from (24) and a pair (x_a^*, w^*) that satisfy (26). The feasible set lies in the half space $\mathcal{H}(g^{(k)}, \lambda^{(k)})$.

V. EXAMPLE

This example considers the robustness of a two link robot arm (Figure 3) as it traverses a finite-time trajectory. This example was previously used to study related finite-horizon robustness issues in [11], [10], [9]. The mass and moment of inertia of the i -th link are denoted by m_i and I_i . The robot properties are $m_1 = 3\text{kg}$, $m_2 = 2\text{kg}$, $l_1 = l_2 = 0.3\text{m}$, $r_1 = r_2 = 0.15\text{m}$, $I_1 = 0.09\text{kg} \cdot \text{m}^2$, and $I_2 = 0.06\text{kg} \cdot \text{m}^2$. The nonlinear equations of motion (Section 2.3 of [1])

Algorithm 1 Ellipsoidal Algorithm

```

1: Given:  $G_a, \epsilon_{tol} > 0, R > 0$ 
2: Initialize:  $\Lambda^{(0)} = R^2 \cdot I, \lambda^{(0)} = 0, J_{bnd} = \infty, k = 0$ 
3: while  $J_{bnd} > \epsilon_{tol}$  do
4:   if  $\lambda_i^{(k)} < 0$  for some  $i$  then
5:      $J(\lambda^{(k)}) = \infty$ 
6:      $g^{(k)} = -e_i$  ( $e_i$  is  $i^{th}$  basis vector).
7:   else
8:     Solve  $RDE(t, Y, \lambda) = 0; Y(T) = 0$ .
9:     if  $Y$  exists on  $[0, T]$  then
10:       $J(\lambda^{(k)}) = \begin{bmatrix} 0 \\ 1 \end{bmatrix}^\top Y(0) \begin{bmatrix} 0 \\ 1 \end{bmatrix}$ 
11:      Compute  $g^{(k)}$  from Theorem 3.
12:    else
13:       $J(\lambda^{(k)}) = \infty$ 
14:      Compute  $g^{(k)}$  from (26) and (24)
15:    end if
16:  end if
17:  Sub-optimality:  $J_{bnd} := \sqrt{(g^{(k)})^\top \Lambda^{(k)} g^{(k)}}$ 
18:  Compute  $(\Lambda^{(k+1)}, \lambda^{(k+1)})$  from (27)
19:  Update iteration number:  $k = k + 1$ 
20: end while

```

are given by:

$$\begin{bmatrix} \alpha + 2\beta \cos(\theta_2) & \delta + \beta \cos(\theta_2) \\ \delta + \beta \cos(\theta_2) & \delta \end{bmatrix} \begin{bmatrix} \ddot{\theta}_1 \\ \ddot{\theta}_2 \end{bmatrix} + \begin{bmatrix} -\beta \sin(\theta_2) \dot{\theta}_2 & -\beta \sin(\theta_2) (\dot{\theta}_1 + \dot{\theta}_2) \\ \beta \sin(\theta_2) \dot{\theta}_1 & 0 \end{bmatrix} \begin{bmatrix} \dot{\theta}_1 \\ \dot{\theta}_2 \end{bmatrix} = \begin{bmatrix} \tau_1 \\ \tau_2 \end{bmatrix} \quad (29)$$

with

$$\alpha := I_1 + I_2 + m_1 r_1^2 + m_2 (l_1^2 + r_2^2) = 0.443 \text{ kg} \cdot \text{m}^2$$

$$\beta := m_2 l_1 r_2 = 0.09 \text{ kg} \cdot \text{m}^2$$

$$\delta := I_2 + m_2 r_2^2 = 0.105 \text{ kg} \cdot \text{m}^2.$$

The state and input are $\eta := [\theta_1 \ \theta_2 \ \dot{\theta}_1 \ \dot{\theta}_2]^T$ and $\tau := [\tau_1 \ \tau_2]^T$, where τ_i is the torque applied to the base of link i . A trajectory $\bar{\eta}$ was selected for the arm and the required input torque $\bar{\tau}$ was computed. Figure 4 shows the desired trajectory for the tip of arm two (red dashed line) in Cartesian coordinates from $t = 0$ to $T = 5$ sec. The arm positions at four different times are

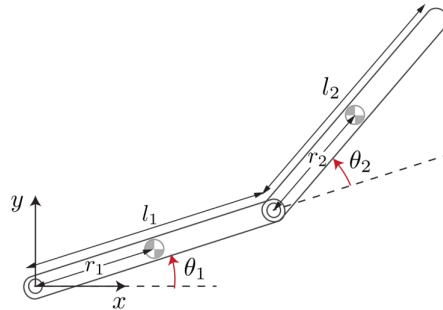


Fig. 3. Two link robot arm [1].

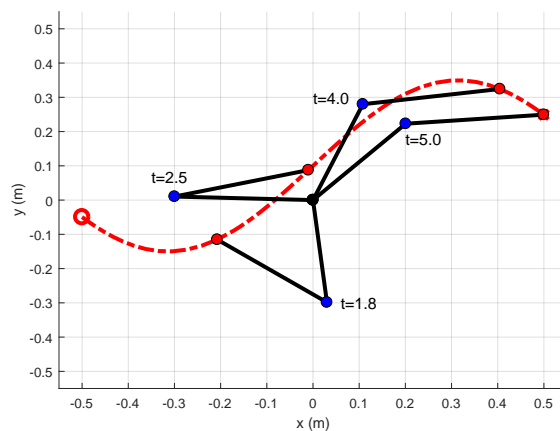


Fig. 4. Desired trajectory in Cartesian coordinates (dotted red line) and robot arm position at four times.

also shown.

A state feedback law is implemented to track this trajectory. The input torque vector is $\tau = \bar{\tau} + u$ where $u(t) = K(t) (\bar{\eta}(t) - \eta(t))$. The feedback gain is constructed via finite horizon, LQR design. Details on the trim trajectory and state feedback design can be found in [10], [9]. Figure 5 shows a block diagram for the uncertain, nonlinear dynamics for the two-link robot and state feedback. The analysis aims to bound the $\mathcal{L}_2[0, T]$ norm of the tracking error $e(t) = \bar{\eta}(t) - \eta(t)$ in the presence of uncertainty in the joint torques.

Algorithm 1 was used to compute bounds on the $\mathcal{L}_2[0, T]$ norm of the tracking error e . The causal, uncertainty is assumed to be a full (2-by-2) with bounded induced $\mathcal{L}_2[0, T]$ norm: $\|\Delta\|_{2 \rightarrow 2} \leq \beta$. The corresponding IQC for this uncertainty is defined by $M = \begin{bmatrix} \beta^2 I & 0 \\ 0 & -I \end{bmatrix}$. The IQC variable λ is a scalar and hence Algorithm 1 reduces to bisection in this case.⁴ Algorithm 1 was

⁴The ellipsoids simplify to intervals for scalar variables. The interval is bisected based on the sign of the subgradient evaluated at the interval center.

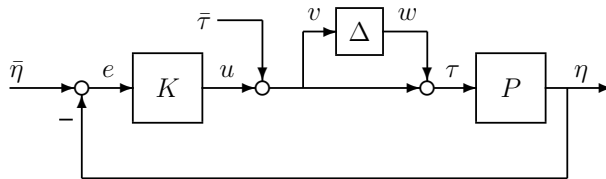


Fig. 5. Uncertain Nonlinear Model for Two-Link Robot

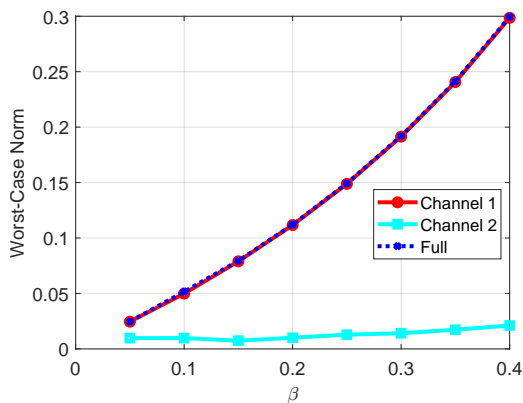


Fig. 6. Worst-case norm versus uncertainty level β for uncertainty structure that is full 2-by-2, on Channel 1 only, and Channel 2 only.

run for uncertainty levels $\beta = 0.05, 0.1, \dots, 0.4$. The bisection was initialized with the interval $[0, 10]$ and was run until the optimality gap was less than 1%. The results are shown by the blue curve in Figure 6. This took ≈ 290 sec for the eight calculations on a standard laptop computer.

The analysis was repeated under two additional assumptions on the uncertainty: (i) uncertainty on channel 1, $\Delta := \begin{bmatrix} \Delta_1 & 0 \\ 0 & 0 \end{bmatrix}$ with $\|\Delta_1\|_{2 \rightarrow 2} \leq \beta_1$, and (ii) uncertainty on channel 2, i.e. $\Delta := \begin{bmatrix} 0 & 0 \\ 0 & \Delta_2 \end{bmatrix}$ with $\|\Delta_2\|_{2 \rightarrow 2} \leq \beta_2$. Define $E_1 = \begin{bmatrix} 1 & 0 \\ 0 & 0 \end{bmatrix}$ and $E_2 = \begin{bmatrix} 0 & 0 \\ 0 & 1 \end{bmatrix}$. The corresponding IQCs for these two uncertainty sets are:

$$(i) M_1 = \begin{bmatrix} \beta_1^2 E_1 & 0 \\ 0 & -E_1 \end{bmatrix}, \quad (ii) M_2 = \begin{bmatrix} \beta_2^2 E_2 & 0 \\ 0 & -E_2 \end{bmatrix}. \quad (30)$$

Algorithm 1 was run for these two cases with same uncertainty levels $\beta_i = 0.05, 0.1, \dots, 0.4$ for $i = 1, 2$. The algorithms again reduces to bisection as each case only has one IQC variable. The bisection was initialized with the interval $[0, 10]$ and was run until the optimality gap was less than 1%. The results are shown by the red and cyan curves in Figure 6. Cases (i) and (ii) took ≈ 240 sec and ≈ 200 sec, respectively. A key observation from these results is that the results for case (i) are very close to those for the full block uncertainty while (ii) results in much smaller

norm. This indicates that uncertainty at the base of link 1 is more significant and uncertainty at the base of link 2 has a negligible effect.

Finally, the analysis was performed with uncertainty in both channels 1 and 2 but no cross-coupling. This corresponds to $\Delta := \begin{bmatrix} \Delta_1 & 0 \\ 0 & \Delta_2 \end{bmatrix}$ with $\|\Delta_i\|_{2 \rightarrow 2} \leq \beta_i$ for $i = 1, 2$. This case has two IQCs defined by M_1 and M_2 in (30) with the corresponding β_i . The analysis was performed with $\beta_1 = 0.05$ and $\beta_2 = 0.8$, i.e. much larger uncertainty in channel 2. Algorithm 1 was initialized with a sphere of radius $R = 20$. The ellipsoid algorithm was run to an optimality gap of 1%. This converged after 51 iterations and took ≈ 95 sec. It converged to $\lambda_1^* = 0.0142$ and $\lambda_2^* = 0.0447$ with $\sqrt{J^*} = 0.139$.

For comparison, the original infinite-dimensional formulation (11) was approximated by: (i) enforcing the DLMI on a grid of 20 evenly spaced time points between $[0, 5]$, (ii) treating $P(t)$ at 10 evenly spaced time points as decision variables, and (iii) using cubic splines to evaluate $P(t)$ and $\dot{P}(t)$ at the DLMI grid points. Solving this (approximate) finite-dimensional SDP gives $\lambda_{1,SDP} = 0.0195$ and $\lambda_{2,SDP} = 0.0448$ with $\sqrt{J^*} \approx 0.147$. We then solved the RDE using these IQC variables and obtained a bound of $\sqrt{J^*} \leq \sqrt{J(\lambda_{SDP})} = 0.140$. Solving the SDP followed by the RDE only took ≈ 6 secs. Thus the standard heuristic (gridding and basis functions) yields a nearly optimal answer with much less computation time on this particular example. However, no optimality gap is provided with this heuristic.

VI. CONCLUSIONS

This paper presented a method to analyze the robustness of an uncertain nonlinear system along a finite-horizon trajectory. The approach relies on a linearization of the nominal nonlinear system along the trajectory. A DLMI condition was then developed using the linearized, uncertain LTV system. This led to an infinite dimensional convex optimization to assess robustness. This optimization was then converted to an equivalent finite dimensional optimization based on a related Riccati Differential Equation. The ellipsoidal method to solve this optimization avoids heuristics often used to solve DLMIs, e.g. time gridding. The approach was demonstrated by a two-link robotic arm example. This included a comparison of the ellipsoid method and heuristic gridding approaches. Future work will include implementations for more general (dynamic, soft) IQCs.

REFERENCES

- [1] R. Murray, Z. Li, and S. Sastry, *A Mathematical Introduction to Robot Manipulation*. CRC Press, 1994.

- [2] A. Marcos and S. Bennani, “LPV modeling, analysis and design in space systems: Rationale, objectives and limitations,” in *AIAA Guidance, Nav., and Control Conf.*, 2009, pp. AIAA 2009–5633.
- [3] F. Biertümpfel, N. Pholdee, S. Bennani, and H. Pfifer, “Finite horizon worst-case analysis of linear time-varying systems applied to launch vehicle,” *arXiv preprint arXiv:2111.12748*, 2021.
- [4] J. Theis, D. Ossmann, F. Thielecke, and H. Pfifer, “Robust autopilot design for landing a large civil aircraft in crosswind,” *Control Engineering Practice*, vol. 76, pp. 54–64, 2018.
- [5] A. Megretski and A. Rantzer, “System analysis via integral quadratic constraints,” *IEEE Transactions on Automatic Control*, vol. 42, no. 6, pp. 819–830, 1997.
- [6] J. Veenman, C. Scherer, and H. Köroğlu, “Robust stability and performance analysis based on integral quadratic constraints,” *European Journal of Control*, vol. 31, pp. 1–32, 2016.
- [7] K. Schweidel, J. Buch, P. Seiler, and M. Arcak, “Computing worst-case disturbances for finite-horizon linear time-varying approximations of uncertain systems,” *IEEE Control Systems Letters*, vol. 5, no. 5, pp. 1753–1758, 2020.
- [8] F. Biertümpfel, J. Theis, and H. Pfifer, “Robustness analysis of nonlinear systems along uncertain trajectories,” in *Submitted to the 2023 IFAC World Congress*, 2022.
- [9] R. Moore, “Finite horizon robustness analysis using integral quadratic constraints,” Master’s thesis, University of California, Berkeley, 2015.
- [10] P. Seiler, R. Moore, C. Meissen, M. Arcak, and A. Packard, “Finite horizon robustness analysis of LTV systems using integral quadratic constraints,” *arXiv:1711.07248*, 2017.
- [11] —, “Finite horizon robustness analysis of LTV systems using integral quadratic constraints,” *Automatica*, vol. 100, pp. 135–143, 2019.
- [12] H. Pfifer and P. Seiler, “Less conservative robustness analysis of linear parameter varying systems using integral quadratic constraints,” *Int. Journal of Robust and Nonlinear Control*, vol. 26, no. 16, pp. 3580–3594, 2016.
- [13] F. Wu, X. H. Yang, A. Packard, and G. Becker, “Induced l2-norm control for lpv systems with bounded parameter variation rates,” *International Journal of Robust and Nonlinear Control*, vol. 6, no. 9-10, pp. 983–998, 1996.
- [14] G. Tadmor, “Worst-case design in the time domain: The maximum principle and the standard H_∞ problem,” *Math. of Control, Signals, and Systems*, vol. 3, pp. 301–324, 1990.
- [15] R. Ravi, K. Nagpal, and P. Khargonekar, “ H_∞ control of linear time-varying systems: A state-space approach,” *SIAM J. of Control and Optim.*, vol. 29, no. 6, pp. 1394–1413, 1991.
- [16] M. Green and D. J. N. Limebeer, *Linear Robust Control*. Prentice Hall, 1995.
- [17] W. Chen and F. Tu, “The strict bounded real lemma for linear time-varying systems,” *Journal of Math. Analysis and Applications*, vol. 244, pp. 120–132, 2000.
- [18] T. Başar and P. Bernhard, *H^∞ Optimal Control and Related Minimax Design Problems*, 3rd ed. Birkhauser, 2008.
- [19] U. Jönsson, “Robustness of trajectories with finite time extent,” *Automatica*, vol. 38, pp. 1485–1497, 2002.
- [20] I. Petersen, V. Ugrinovskii, and A. Savkin, *Robust Control Design Using H^∞ Methods*. Springer, 2000.
- [21] C.-Y. Kao, A. Megretski, and U. Jonsson, “A cutting plane algorithm for robustness analysis of periodically time-varying systems,” *IEEE Transactions on Automatic Control*, vol. 46, no. 4, pp. 579–592, 2001.
- [22] D. A. Jaoude and M. Farhood, “Customized analytic center cutting plane methods for the discrete-time integral quadratic constraint problem,” *IFAC-PapersOnLine*, vol. 55, no. 25, pp. 115–120, 2022.
- [23] J. Fry, M. Farhood, and P. Seiler, “IQC-based robustness analysis of discrete-time linear time-varying systems,” *International Journal of Robust and Nonlinear Control*, vol. 27, no. 16, pp. 3135–3157, 2017.
- [24] M. Palframan, J. Fry, and M. Farhood, “Robustness analysis of flight controllers for fixed-wing unmanned aircraft systems using integral quadratic constraints,” *IEEE Trans. on Control Systems Tech.*, 2017.

- [25] K. Zhou, J. C. Doyle, and K. Glover, *Robust and Optimal Control*. Prentice-Hall, 1996.
- [26] B. Takarics and P. Seiler, “Gain scheduling for nonlinear systems via integral quadratic constraints,” in *American Control Conference*, 2015, pp. 811–816.
- [27] A. van der Schaft, *L_2 -gain and passivity in nonlinear control*. Springer-Verlag New York, Inc., 1999.
- [28] J. Willems, “Dissipative dynamical systems part I: General theory,” *Arch. for Rational Mech. and Analysis*, vol. 45, no. 5, pp. 321–351, 1972.
- [29] —, “Dissipative dynamical systems part II: Linear systems with quadratic supply rates,” *Arch. for Rational Mech. and Analysis*, vol. 45, no. 5, pp. 352–393, 1972.
- [30] H. Khalil, *Nonlinear Systems*, 3rd ed. Prentice Hall, 2001.
- [31] S. Boyd, L. E. Ghaoui, E. Feron, and V. Balakrishnan, *Linear Matrix Inequalities in System and Control Theory*, ser. Studies in Applied Math. SIAM, 1994, vol. 15.
- [32] B. Anderson and J. Moore, *Optimal control: linear quadratic methods*. Courier Corporation, 2007.
- [33] A. Iannelli, P. Seiler, and A. Marcos, “Construction of worst-case disturbances for LTV systems with application to flexible aircraft,” *Submitted to the AIAA Journal of Guidance, Control, and Dynamics*, 2018.
- [34] S. Boyd and C. Barratt, *Linear controller design: limits of performance*. Citeseer, 1991, vol. 7.
- [35] R. Bitmead and M. Gevers, *The Riccati Equation*. Springer Science & Business Media, 2012, ch. 10. Riccati Difference and Differential Equations: Convergence, Monotonicity, and Stability.
- [36] A. Czornik, “Continuity of the solution of the Riccati equations for continuous time JLQP,” *IEEE Transactions on Automatic Control*, vol. 45, no. 5, pp. 934–937, 2000.
- [37] M. Vidyasagar, *Nonlinear systems analysis*. SIAM, 1993.

APPENDIX

The main text denoted the Riccati Differential Equation by $RDE(t, Y) = 0$ (dropping any dependence on λ). This appendix focuses on the case where the right side is a matrix function of time $W : [0, T] \rightarrow \mathbb{S}^{n_x+1}$. Specifically, $RDE(t, Y) = W$ denotes the following RDE:

$$\begin{aligned} \dot{Y} + A_a^\top Y + Y A_a + Q \\ - (Y B_a + S) R^{-1} (Y B_a + S)^\top = W \end{aligned} \tag{31}$$

This appendix provides supporting lemmas regarding the monotonicity and continuity of the RDE solutions under such perturbations.

Lemma 1. *Assume:*

- 1) $R(t) \prec 0$ for all $t \in [0, T]$
- 2) $W_i : [0, T] \rightarrow \mathbb{S}^{n_x+1}$ are functions ($i = 1, 2$) that satisfy $W_1(t) \preceq W_2(t) \forall t \in [0, T]$.
- 3) $Y_i : [0, T] \rightarrow \mathbb{S}^{n_x+1}$ are differentiable functions ($i = 1, 2$) that satisfy $Y_1(T) \succeq Y_2(T)$ and $RDE(t, Y_i) = W_i \forall t \in [0, T]$.

Then $Y_1(t) \succeq Y_2(t) \forall t \in [0, T]$.

Proof. Define the difference as $E := Y_1 - Y_2$ and note that $E(T) \succeq 0$. Subtract $RDE(t, Y_2) = W_2$ from $RDE(t, Y_1) = W_1$ to obtain, after some algebra, the following expression:

$$\dot{E} + \hat{A}^\top E + E\hat{A} = F$$

where

$$\begin{aligned}\hat{A} &:= A_a - B_a R^{-1} (Y_2 B_a + S)^\top, \\ F &:= W_1 - W_2 + E B_a R^{-1} B_a^\top E.\end{aligned}$$

The assumptions on W_1 , W_2 , and R imply that $F(t) \preceq 0$ for all $t \in [0, T]$. Next, let $\Phi(t, \tau)$ be the state transition matrix associated with $\dot{x}(t) = -\hat{A}^\top(t)x(t)$. By Lemma 10.3 in [35], the solution E can be expressed as:

$$\begin{aligned}E(t) &= \Phi(t, T) E(T) \Phi(t, T)^\top \\ &\quad - \int_t^T \Phi(t, \tau) F(\tau) \Phi(t, \tau)^\top d\tau\end{aligned}\tag{32}$$

Equation 32 implies that $E(t) = P(t) - Y(t) \succeq 0$ because $E(T) \succeq 0$ and $F(t) \preceq 0 \forall t \in [0, T]$. Hence $Y_2(t) \succeq Y_1(t) \forall t \in [0, T]$. \square

Lemma 2. Assume (A_a, B_a, Q, R, S) are all continuous functions of time. Moreover, assume:

- 1) $R(t) \prec 0$ for all $t \in [0, T]$
- 2) $Y_0 : [0, T] \rightarrow \mathbb{S}^{n_x+1}$ is a differentiable function satisfying $Y_0(T) = 0$ and $RDE(t, Y_0) = 0 \forall t \in [0, T]$.
- 3) $\{\epsilon_k\}_{k=1}^\infty \subset \mathbb{R}$ are positive scalars satisfying $\epsilon_k \geq \epsilon_{k+1} \forall k$ and $\lim_{k \rightarrow \infty} \epsilon_k = 0$.
- 4) $Y_k : [0, T] \rightarrow \mathbb{S}^{n_x+1}$ are differentiable functions ($k = 1, 2, \dots$) that satisfy $Y_k(T) = 0$ and $RDE(t, Y_k) = -\epsilon_k \cdot I \forall t \in [0, T]$.

Then $\lim_{k \rightarrow \infty} \|Y_k(t) - Y_0(t)\| = 0 \forall t \in [0, T]$.

Proof. The proof adapts similar arguments used to prove Theorem 3 in [36]. First, the horizon is finite $T < \infty$ and $[0, T]$ is a compact set. Hence the solution Y_1 is uniformly bounded, i.e. there exists $c_1 < \infty$ such that:

$$\max_{t \in [0, T]} \|Y_1(t)\| \leq c_1\tag{33}$$

where $\|Y_1(t)\|$ is the (matrix) induced 2-norm of $Y_1(t)$. By Lemma 1, $Y_1(t) \succeq Y_0(t)$ and $Y_1(t) \succeq Y_k(t)$ ($k = 2, 3, \dots$) for all $t \in [0, T]$. Thus Y_0 and $\{Y_k\}_{k=2}^\infty$ are also uniformly bounded by c_1 .

Next, define $E_k := Y_k - Y_0$ and note that $E_k(T) = 0$. Moreover, define:

$$\begin{aligned}\hat{A} &:= A_a - B_a R^{-1}(Y_0 B_a + S)^\top, \\ F_k &:= -\epsilon_k I + E_k B_a R^{-1} B_a^\top E_k.\end{aligned}$$

Following the same arguments as in the proof of Lemma 1, the solution E_k can be expressed as:

$$E_k(t) = - \int_t^T \Phi(t, \tau) F(\tau) \Phi(t, \tau)^\top d\tau, \quad (34)$$

where $\Phi(t, \tau)$ is the state transition matrix for $-\hat{A}^\top$. The state transition matrix is also uniformly bounded: $\exists c_2$ such that $\|\Phi(t, \tau)\| \leq c_2 \forall t, \tau \in [0, T]$. Moreover, $\exists c_3$ such that $\|B_a(t)R^{-1}(t)B_a(t)\| \leq c_3$ for all $t \in [0, T]$. Use these constants and (34) to bound E_k as follows:

$$\begin{aligned}\|E_k(t)\| &\leq \int_t^T c_2^2 (\epsilon_k + c_3 \|E_k(\tau)\|^2) d\tau \\ &\leq c_2^2 \epsilon_k T + \int_t^T 2c_1 c_2^2 c_3 \|E_k(\tau)\| d\tau\end{aligned}$$

where the second line follows from $\|E_k(\tau)\| \leq \|Y_k(\tau)\| + \|Y_0(\tau)\|$ combined with the uniform bound c_1 defined above. Apply Grönwall's inequality (Lemma 1 in Section 5.7 of [37]) to obtain:

$$\|E_k(t)\| \leq c_2^2 \epsilon_k T \cdot e^{2c_1 c_2^2 c_3 (T-t)} \quad (35)$$

Finally, $\lim_{k \rightarrow \infty} \epsilon_k = 0$ implies that $\lim_{k \rightarrow \infty} \|E_k(t)\| = 0$ for all $t \in [0, T]$. \square